ELSEVIER

Physica C 234 (1994) 311–317

PHYSICA C

Angular dependence of the magnetic properties of thin $YBa_2Cu_3O_{7-\delta}$ films irradiated with Pb and Xe ions

R. Prozorov [a,*], A. Tsameret [a], Y. Yeshurun [a], G. Koren [b], M. Konczykowski [c], S. Bouffard [d]

[a] *Department of Physics, Bar-Ilan University, 52900 Ramat-Gan, Israel*
[b] *Department of Physics, Technion, Haifa, Israel*
[c] *Laboratoire des Solides Irradiés, Ecole Polytechnique, 91128 Palaiseau Cedex, France*
[d] *Centre Interdisciplinaire de Recherches avec les Ions Lourds, P.B. 5133, 14040 Caen Cedex, France*

Received 26 September 1994; revised manuscript received 18 October 1994

Abstract

We study the angular dependence of the magnetic properties of Y–Ba–Cu–O thin films irradiated with 0.86 GeV Pb and 5 GeV Xe ions. For the Pb irradiated samples the critical current has a maximum when the direction of the external magnetic field coincides with the direction of the columnar defects induced by the irradiation. For the Xe irradiated samples such anisotropy in the critical current was not found. The pinning force density obeys a scaling law of the form $b^p(1-b)^q$, where $b=H_{ext}/H_{irr}(T)$, and H_{ext} and H_{irr} are the external and the irreversibility fields, respectively. The exponents p and q depend on the type and direction of the irradiation.

1. Introduction

The introduction of artificial defects has proved to be a very important tool in increasing the efficiency of flux pinning, and thus the critical current density, in high-T_c superconductors (HTS's). A very useful way to produce pinning centers in a controlled way is by irradiation with heavy ions [1–6]. The advantage of this method is the ability to produce pinning centers of well defined size, orientation and concentration. The micro-structure of the defects introduced by the irradiation depends on the kind of ion used in the irradiation, the energy of the ions and the dose of irradiation. In particular, high-energy (several GeV) Pb irradiation introduces columnar defects, whereas Xe ions produce point-like and cluster-like defects [1–3]. Extensive studies of HTS crystals show that columnar defects produced by Pb irradiation serve as efficient pinning centers with unidirectional features [5], namely that the critical current, deduced from the width of the magnetization curves reaches the maximum when the flux lines are aligned along the direction of the irradiation.

The study of superconductors with artificial pinning centers is of particular interest for thin films, which are more favorable than crystals for practical applications. In spite of an intensive experimental study of irradiation effects on thin films of copper-oxide superconductors (see e.g. Ref. [2]), the angular dependence of the critical current was hardly examined. The only exception we are aware of is a recent work by Holzapfel et al. [6], who have studied the angular dependence of the *transport* critical current in thin films irradiated with heavy ions.

In this paper we report on the angular dependence of the *magnetic* properties in YBCO thin films irra-

* Corresponding author.

SSDI 0921-4534(94)02319-0

diated with Pb and Xe. The results show that in films irradiated with Pb ions, where columnar defects are manifest, a unidirectional enhancement of the critical current along the direction of irradiation is observed, similar to the effect which has been observed in crystals [5]. In films irradiated with Xe ions, however, this effect was not found.

2. Experimental

Thin YBCO films were laser ablated on [100] MgO and $SrTiO_3$ substrates, as described in detail in Ref. [7]. The films were irradiated by either 0.86 GeV Pb^{+53} or 5 GeV Xe^{+44} ions along either the c direction or at 45° relative to it. The irradiation was carried out at the Grand Accélérateur National d'Ions Lourds (GANIL, Caen, France). The Pb^{+53} ions produce continuous cylindrical amorphous tracks along their path with a diameter of about 7 nm. The Xe^{+44} ions, on the other hand, do not produce columnar defects, but rather clusters of point-like defects, which are dispersed around the ions' trajectories [1–3]. Information related to our samples and details of irradiation are found in Table 1.

All measurements presented below were performed on an Oxford-Instruments vibrating sample magnetometer (VSM), which allows for rotation of a sample relative to the direction of the external magnetic field. We denote the angle between the direction of the irradiation and c-axis by θ, and the angle between the direction of the external magnetic field and the c-axis by φ. We note that in VSM we measure the component of the magnetic moment along the magnetic field. In order to correct for the fact that the magnetization vector points in the c direction in the films, the measured magnetic moment is divided by $\cos(\varphi)$ to yield the actual moment M.

3. Results

3.1. Unidirectional anisotropy

3.1.1. Pb irradiation

Fig. 1 shows a typical set of magnetization curves, at 44 K, for sample F11 (irradiated with Pb ions along $\theta = +45°$) for various φ. The width ΔM of the magnetization loops increases with the increase of angle from $\varphi = -45°$ to $+45°$. The maximum width is for the loop measured for $\varphi = +45°$, namely when the external field is along the direction of the irradiation. The critical current density J_c was derived from the width of such magnetization curves (at the given temperature and field) using the sand-pile model [8], which gives, in the case of a rectangle of sides $a \leq b$, $J_c = 20\Delta M/(a^2 bt(1 - a/(3b)))$, where t is the thickness of the film. We assume that the shielding current density is constant across the thin film [9] and, hence, we use the above formula considering the film as a cross-section of an infinite slab. We note that for our films this model yields J_c values which are somewhat smaller than those obtained, for similar films, in transport measurements. At this stage it is not clear to us whether this difference reflects the creep process or deterioration of the films because of aging or irradiation.

Fig. 2 summarizes the derived critical current density J_c at $T = 64$ K as a function of the angle φ for sample F11. The figure demonstrates a distinctive angular anisotropy of J_c with a sharp peak at $\varphi = 45°$, consistent with the transport data of Ref. [9]. It is quite clear that without columnar defects, the direction $\varphi = 45°$ is exactly equivalent to the direction $\varphi = -45°$, and therefore any difference in the magnetic behavior between these directions is due to an interaction between the vortices and the columnar defects.

Table 1
Information on the samples studied. θ is the angle of irradiation with respect to the c-axis (which is perpendicular to the plane of the film)

Name	Dimensions (cm^2)	Thickness (nm)	Substrate	Ion	θ	T_c (K)
VA	0.400×0.430	200	MgO	unirr.	unirr.	89.5
F4	0.471×0.162	225	MgO	Pb^{+53}	0°	83.5
F11	0.709×0.325	300	$SrTiO_3$	Pb^{+53}	45°	83.5
B13	0.630×0.320	300	$SrTiO_3$	Xe^{+44}	45°	88.5

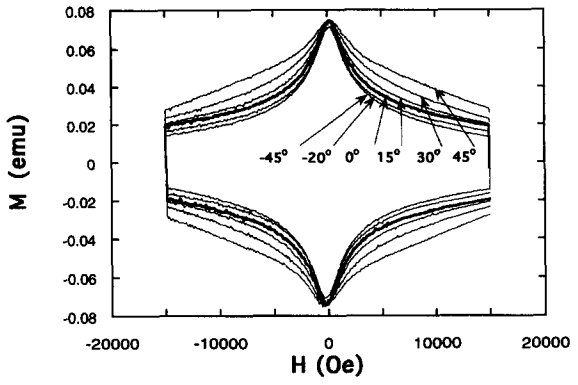

Fig. 1. Magnetization loops for sample F11 ($\theta=+45°$) at $T=44$ K for the indicated angles $\varphi=-45°$, $-20°$, $0°$, $15°$, $30°$ and $45°$.

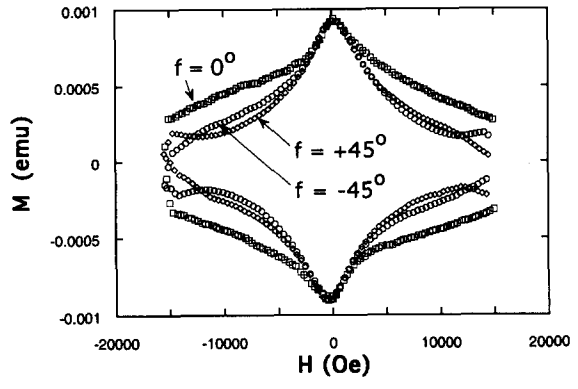

Fig. 3. Magnetization loops for sample F4 ($\theta=0°$) at $T=34$ K for different angles $\varphi=-45°$, $0°$ and $45°$.

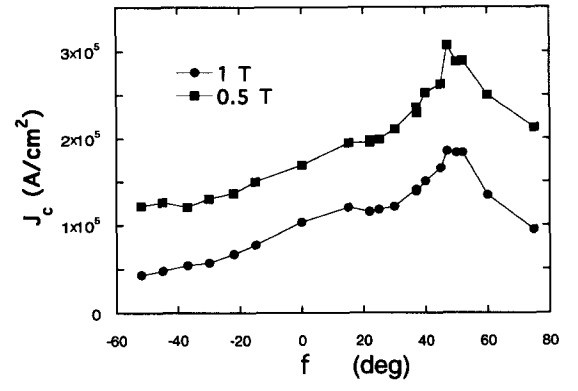

Fig. 2. Angular dependence of the critical current density for sample F11 ($\theta=+45°$) at $T=64$ K for two values of the external magnetic field: $H=0.5$ T (squares) and 1 T (circles). Note the peak at $\varphi=+45°$. The lines are guides for the eye.

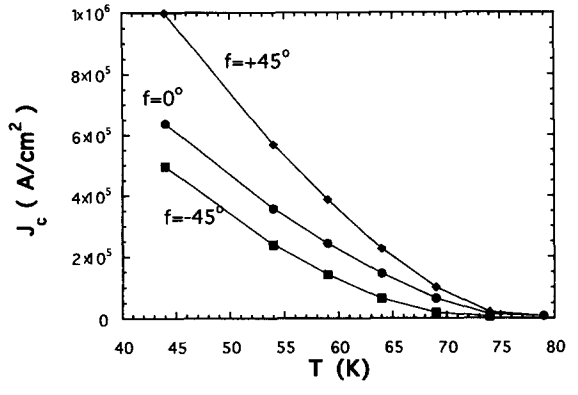

Fig. 4. Temperature dependence of the critical current density for sample F11 ($\theta=+45°$) for different angles $\varphi=-45°$, $0°$ and $45°$ at the external field $H=1$ T.

A similar pinning anisotropy was observed for films that were irradiated by Pb ions along $\theta=0°$. Fig. 3 shows magnetization curves for sample F4, for $\varphi=-45°$, $0°$ and $+45°$. The curves measured at $\pm 45°$ are almost identical, whereas the width of the curve for the field along the irradiation direction shows a substantial increase for sufficiently large fields.

Figs. 1 and 3 show that the magnetic moment is independent of the direction of external magnetic field in the vicinity of $H=0$, so that the loops coincide for all angles φ. This indicates that close to $H=0$ the spatial distribution of the trapped magnetic flux is the same for all φ.

Another demonstration of the anisotropic enhancement of the critical current is presented in Fig. 4. In this figure the critical current, obtained from the widths of magnetization curves at $H=1$ T, is plotted versus temperature for three angles $\varphi=-45°$, $0°$ and $+45°$ for sample F11. It is apparent that the unidirectional pinning is more pronounced for low temperatures, and that it exists almost to the transition temperature.

3.1.2. Xe irradiation

As can be seen from Fig. 5, the samples irradiated with Xe ions do not show a unidirectional enhancement of flux pinning. The figure presents magnetization loops for sample B13 (irradiated by Xe ions along $\theta=+45°$), for $\varphi=-45°$ and $+45°$, at $T=64$ K. The magnetization loops are almost identical. Such φ independent magnetization was observed between 64 K (the lowest temperature in our experiments), and

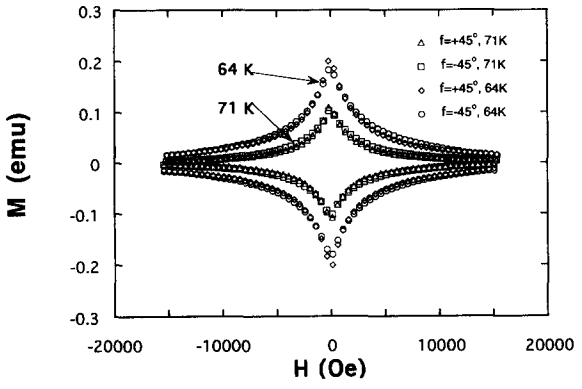

Fig. 5. Magnetization loops for sample B13 ($\theta=+45°$) at $T=64$ K and 71 K for the angles $\varphi=-45°$ and 45°.

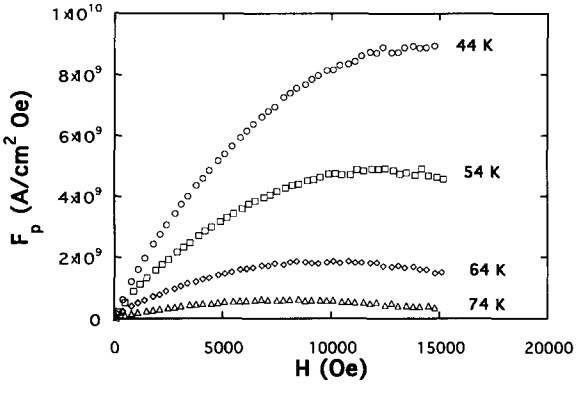

Fig. 6. The pinning-force density as a function of magnetic field for sample F11 ($\theta=+45°$), for $\varphi=+45°$, at different temperatures $T=44$, 54, 64 and 74 K.

$T=76$ K (above which the signal is too weak to be reliably recorded).

3.2. Pinning force

A powerful method to analyze the mechanism of pinning is the study of the pinning-force density $F_p=|J_c\times H_{ext}|$ (we assume $B=H_{ext}$), as a function of temperature and magnetic field [8]. The functional form of F_p may provide insight into the pinning mechanism for different samples. It is important to note that unlike conventional superconductors, F_p in HTS's depends on the time-window of the experiment and it is therefore denoted below as the *apparent* pinning force $F_{p,ap}=|J\times H_{ext}|$, where $J<J_c$ because of flux creep.

Fig. 6 shows the pinning force as a function of the magnetic field for sample F11, in the case when the magnetic field is aligned along the direction of the defects ($\varphi=45°$), for various temperatures. Fig. 7 shows scaling of the pinning force, obtained by using the variables $F^*=F_{p,ap}/F_m$ and $b^*=H/H_m$, where $F_m(T)$ is the maximal value of $F_{p,ap}(T, H)$ and H_m is the magnetic field value at $F_{p,ap}=F_m$. The scaled pinning forces for the sample F4 ($\theta=0°$, $\varphi=0°$) coincide with that for F11 ($\theta=45°$, $\varphi=45°$), indicating a common pinning mechanism in both cases. The scaled pinning force of the samples B13 (Xe irradiated at $\theta=45°$), F11 (Pb irradiated at $\theta=45°$, for two directions of the magnetic field), F4 (Pb irradiated at $\theta=0°$), and VA (unirradiated) are shown together in Fig. 8.

4. Discussion

The general impression of our data is that Pb irradiated films and crystals exhibit a similar unidirectional magnetic anisotropy despite the fact that the thickness of our films is comparable with the London penetration depth λ. We note, however, that for Xe irradiated films we did not observe unidirectional anisotropy. The different behavior may be understood by the difference in the micro-structure of the defects resulting from the irradiation. The Pb ions produce continuous columnar defects, whereas the Xe ions produce non-continuous defects in the form of clusters along the direction of the irradiation [1–3].

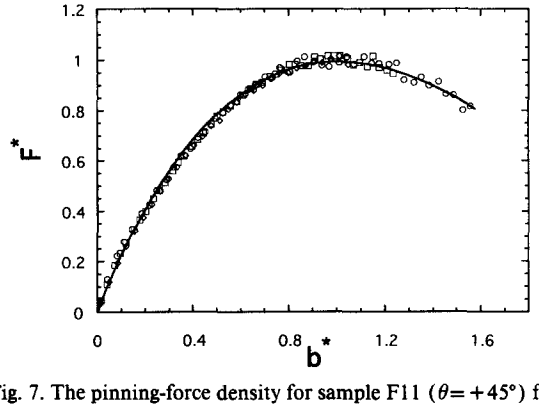

Fig. 7. The pinning-force density for sample F11 ($\theta=+45°$) for $\varphi=+45°$, normalized with the peak coordinates H_m and F_m at $T=44$, 54 and 64 K. The solid curve is a fit by $F^*=2.17b^{*0.96}(1-0.323b^*)^2$.

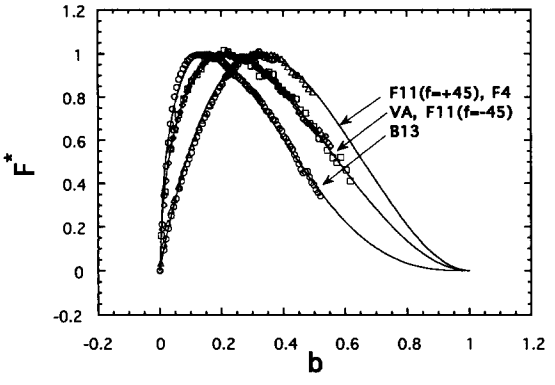

Fig. 8. The pinning force density for samples: F11 ($\theta=+45°$) for $\varphi=+45°$ and $-45°$; F4 ($\theta=0°$) for $\varphi=0°$; B13 ($\theta=+45°$) and VA (unirradiated), in normalized coordinates, according to Eq. (1). The solid curves are corresponding fits (see text).

We note that Holzapfel et al. [6] did observe a unidirectional pinning in thin films irradiated by Xe ions. However, they used Xe ions with smaller energies (0.34 GeV). The energy deposition rate S_e for the Xe ions reaches a maximum at about 1 GeV [1], and therefore it is probable that the Xe irradiation in the experiment of Holzapfel et al. actually produced columnar defects.

The scaling analysis of the pinning force enables us to compare the different samples with respect to the type of irradiation and the external field direction. In most cases, for both conventional [10] and high-T_c superconductors [11], the pinning force obeys a scaling law which can be written as

$$F_{p,ap}(T, H_{ext}) = F(T) b^p (1-b)^q . \qquad (1)$$

Here $F(T)$ is a function which depends only on the temperature, and b is a normalized field H_{ext}/H_0, where H_0 is some scaling field. The exponents p and q depend on the type of pinning centers and elastic properties of the flux-line lattice (FLL) [10,11]. In conventional superconductors, where thermal fluctuations are rather negligible, H_{c2} is used as the scaling field H_0. However, in high-T_c superconductors one should use the irreversibility field H_{irr} as the scaling field [11]. This choice of the scaling field is justified by the fact that H_0 is, by virtue of Eq. (1), the field at which $F_{p,ap}$ becomes zero. This (time-dependent) field is, by definition, H_{irr}. A number of reports confirm the scaling law of Eq. (1) with $H_0=H_{irr}$ [12–14].

The data of Fig. 7 and also previous experimental works [14–16], imply a modified scaling function:

$$F_{p,ap}(T, H_{ext}) = F_m(T) K b^{*p} (1-ab^*)^q , \qquad (2)$$

where $F_m(T)$ is the (time-dependent) maximum value of $F_{p,ap}(T, H)$; K and a are parameters that are independent of the field and temperature; $b^*=H/H_m$ is a scaled field, where H_m is the magnetic field value at $F_{p,ap}=F_m$. We now assume that the pinning force obeys the scaling law in the form of Eq. (1) in the whole range of fields $b=0$ to 1. This assumption is not always valid; for example, a scaling in the form of Eq. (2) was observed in BSCCO crystals [15] only up to H_m, but not in the whole range of b. This implies that in that case there was no scaling in the form of Eq. (1). However, if $F_{p,ap}$ is scaled with H_{irr}, it is also scaled with H_m, under the substitution of $a=H_m/H_{irr}$ and $F_mK=F(T)(H_m/H_{irr})^p$ in Eq. (2).

Thus, such an analysis allows us to obtain, in an indirect way, the irreversibility field $H_{irr}(T)$. For example, a fit to the curve in Fig. 7 yields the parameter $a=H_m/H_{irr}=0.323$ for the sample F11, in the case of $\varphi=45°$. The data can now be scaled by Eq. (1) and we find $H_{irr}(T)$ from the measured $H_m(T)$. Fig. 9 shows the temperature dependence of the H_{irr} derived in such a way for $\varphi=\pm45°$, for sample F11. Conventionally, H_{irr} is defined from the magnetization curves as the field above which the ascending and the descending branches of $M(H)$ coincide. From the

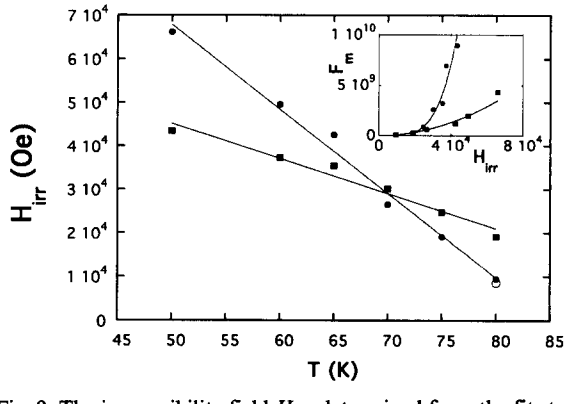

Fig. 9. The irreversibility field H_{irr}, determined from the fits to the pinning-force density, as a function of temperature, for sample F11 ($\theta=+45°$) for $\varphi=+45°$ (solid circles) and $\varphi=-45°$ (squares). The open circle is a direct measurement of H_{irr} for F11 at 74 K. Inset: The peak value F_m as a function of H_{irr} for $\varphi=+45°$ and $-45°$.

magnetization curve at 74 K we found $H_{irr}=0.85$ T (open circle in Fig. 9), in good agreement with the value obtained from the fit. We could not reach H_{irr} for lower temperatures because of the limitation in the magnetic field (1.5 T) in the experiment. In the inset of Fig. 9 F_m is plotted versus $H_{irr}=H_m/a$, for the two angles $\varphi=-45°$ and $+45°$. A power law $F_m=KH_{irr}^{\gamma}$ is obtained. A best fit gives for the exponent $\gamma=2$ and 4.3 for the angles $\varphi=-45°$ and 45°, respectively.

The presentation of $F_{p,ap}$ in the form suggested by Eq. (1) makes it possible to compare directly different samples with respect to the pinning efficiency. As shown in Fig. 8, there are three different functional forms of $F_{p,ap}$:

(1) for the Pb irradiated samples F11 and F4 with the direction of the external field along the columnar defects $F^*=6.45b^{0.96}(1-b)^2$, and the value of b at F^* (max) $b_m=1/3$;

(2) for F11 with the field perpendicular to the defects, and for the virgin sample $F^*=3.82b^{0.55}(1-b)^2$, $b_m=0.22$;

(3) for the Xe irradiated sample B13 $F^*=4.64b^{0.55}(1-b)^3$, $b_m=0.15$. The different functional form of the scaled pinning force, which is manifest in the parameters p, q and the peak position b_m in Eq. (1), reflects different types of pinning mechanisms, associated with different defects in our samples.

It is important to note that the straightforward relationship between $F_{p,ap}$ and the pinning mechanism is relevant only in the shortest time scale, before relaxation affects the value of the critical current. However, we believe that the original pinning force F_p (at $t=0$) will collapse to the same universal curve together with scaled pinning forces $F_{p,ap}$ taken at the later times. To justify such an approach we note that our preliminary relaxation experiments on the irradiated films showed weaker flux creep than that found in irradiated YBCO crystals [17]. This allows us to consider J as constant on the scale of our time-window. Moreover, recent creep measurements in YBCO crystals [15] demonstrate that $F_{p,ap}$ exhibits the same scaling behavior for all experimental time windows. These scaling features are probably related to a field independence of the relaxation rate in a certain range of fields. From the point of view of the collective pinning theory, such a situation occurs in the single-vortex pinning regime. For the case of thin films (where pinning is rather strong) it has been established [18] that this regime is maintained for fields up to 1 T and temperatures up to 80 K. Our measurements are thus performed in the single vortex regime. Therefore, the scaling of $F_{p,ap}$ can provide us with important information about the particular pinning mechanism in the films.

The origin of the pinning mechanism in the different cases can be speculated on phenomenologically in view of several studies of the scaled pinning force that were carried out recently for high-T_c superconductors. Taking into account the creep phenomena, Niel [11] calculated the pinning force for different types of pinning centers and found that $p=\frac{1}{2}$, $q=2$ describe pinning by a surface. Quite similar exponents ($p=0.6$ and $q=2.2$) were found experimentally by Juang et al. [19] for unirradiated Tl–Ba–Ca–Cu–O thin films. They suggested that this functional form of $F_{p,ap}$ makes surface core pinning manifest. As shown above, the pinning force, in the case of the Pb irradiation where the field direction is perpendicular to the direction of irradiation, exhibits the same pinning mechanism as that of the unirradiated sample, with the exponents $p\approx\frac{1}{2}$, $q=2$. It is therefore plausible that this form of $F_{p,ap}$ is due to pinning on planar defects, which always exist in laser-ablated films.

The sample B13 (irradiated with Xe along $\theta=+45°$) makes manifest a pinning mechanism which differs from the virgin sample, with $q=3$ instead of 2. It was suggested that the exponent $q=3$ arises from a combined effect of the shear modulus C_{66} and the tilt modulus C_{44}, in contrast to a dominant shear motion of the FLL in the case of $q=2$ [10].

In order to obtain a full understanding of the relationship between the functional form of the pinning force and the pinning mechanism one should take into account many different factors such as the behavior of elastic constants of the flux-line lattice, the interaction of a vortex with a pinning center [10–13,16], the understanding of which is still incomplete, especially in the case of highly anisotropic superconductors.

Concluding, we have presented a first study of the angular dependence of the magnetization of YBCO thin films irradiated with high-energy Pb and Xe ions. The Pb irradiated samples exhibit a unidirectional anisotropy of the critical current, so that J_c reaches

Table 2
Scaling exponents p and q according to Eq. (1) for different types of defects

Type of defects in thin film	p	q
As-grown defects (e.g. grain boundaries)	0.55	2
Discontinuous clusters (after Xe irradiation)	0.55	3
Columnar defects (after Pb irradiation)	0.96	2

maximum when the direction of the external magnetic field coincides with the direction of the irradiation. On the other hand, the Xe irradiated samples did not show such anisotropy. These results demonstrate that different types of defects make different contributions to the pinning force $F_{p,ap}$. The differences in the pinning efficiency for the various samples and the dependence on the direction of the external magnetic field were clearly reflected in the functional form of $F_{p,ap}$ when scaled with H_{irr}. The scaling exponents are summarized in Table 2.

Acknowledgements

This project has been jointly supported by an International Cooperation Grant of the European Union under contract number CI-1-CT93-0069 and the Israeli Ministry of Science and the Arts.

References

[1] V. Hardy, D. Groult, M.Y. Hervieu, J. Provost, B. Raveau and S. Bouffard, Nucl. Instr. and Meth. B 54 (1991) 472.
[2] M.P. Siegal, R.B. van Dover, J.M. Phillips, E.M. Gyorgy, A.E. White and J.H. Marshall, Appl. Phys. Lett. 60 (1992) 2932.
[3] W. Gerhauser, G. Ries, H.W. Neumüller, W. Schmidt, O. Eibel, G. Saemann-Ischenko and S. Klaumünzer, Phys. Rev. Lett. 68 (1992) 879;
T. Schuster, M.R. Koblischka, H. Kuhn, H. Kronmüller, M. Leghissa, W. Gerhauser, G. Saemann-Ischenko, H.W. Neumüller and S. Klaumünzer, Phys. Rev. B 46 (1992) 8496.
[4] L. Civale, A.D. Marwick, T.K. Worthington, M.A. Kirk, J.R. Thompson, L. Krusin-Elbaum, Y. Sun, J.R. Clem and F. Holtzberg, Phys. Rev. Lett. 67 (1991) 648;
J.R. Thompson, Y.R. Sun, H.R. Kerchner, D.K. Christen, B.C. Sales, B.C. Chakoumakos, A.D. Marwick, L. Civale and J.O. Thomson, Appl. Phys. Lett. 60 (1992) 2306.
[5] L. Klein, E.R. Yacoby, Y. Yeshurun, M. Konczykowski and K. Kishio, Phys. Rev. B 48 (1993) 3523;
L. Klein, E.R. Yacoby, Y. Yeshurun, M. Konczykowski, F. Holtzberg and K. Kishio, Physica C 209 (1993) 251.
[6] B. Holzapfel, G. Kreiselmeyer, M. Kraus, G. Saemann-Ischenko, S. Bouffard, S. Klaumünzer and L. Schultz, Phys. Rev. B 48 (1993) 600.
[7] G. Koren, E. Polturak, B. Fisher, D. Cohen and G. Kimel, Appl. Phys. Lett. 50 (1988) 2330.
[8] A.M. Campbell and J.E. Evetts, Critical currents in superconductors (Taylor & Francis, London, 1972).
[9] V.K. Vlasko-Vlasov, M.V. Indenbom, V.I. Nikitenko, A.A. Polyanskii, R.L. Prozorov, I.V. Grekhov, L.A. Delimova, I.A. Liniichuk, A.V. Antonov and M.Yu. Gusev, Sverkhprovodimost' (SPCT) 5 (1992) 1637;
E.H. Brandt and M.V. Indenbom, Phys. Rev. B 48 (1993) 12893.
[10] E.D. Kramer, J. Appl. Phys. 44 (1973) 1360;
D. Dew-Huges, Philos. Mag. 30 (1974) 293.
[11] L. Niel, Cryogenics 32 (1992) 975.
[12] H. Yamasaki, K. Endo, S. Kosaka, M. Umeda, S. Yoshida and K. Kajimura, Phys. Rev. Lett. 70 (1993) 3331.
[13] L.W. Song, M. Yang, E. Chen and Y.H. Kao, Phys. Rev. B 45 (1992) 3083.
[14] L. Civale, M.W. McElfresh, A.D. Marwick, F. Holtzberg, C. Feild, J.R. Thompson and D.K. Christen, Phys. Rev. B 43 (1991) 13732.
[15] L. Klein, E.R. Yacoby, Y. Yeshurun, A. Erb, G. Mueller-Vogt, V. Breit and H. Wuehl, Phys. Rev. B 49 (1994) 4403.
[16] Z.X. Shi, H.L. Ji, X. Jin, X.X. Yao, X.S. Rong, X.G. Qui and Z. Li, Physica C 215 (1993) 439.
[17] M. Konczykowski, V.M. Vinokur, F. Rullier-Albenque, Y. Yeshurun and F. Holtzberg, Phys. Rev. B 47 (1993) 5531.
[18] R. Griessen, Proc. Int. Workshop on Critical Currents, Austria, 1994.
[19] J.Y. Juang, S.J. Wang, T.M. Uen and Y.S. Gou, Phys. Rev. B 46 (1992) 1188;
R.C. Budhani, M. Suenaga and H. Liou, Phys. Rev. Lett. 69 (1992) 3816.